Non-Equilibrium Phonon Distributions in Sub-100 nm Silicon Transistors

S. Sinha
Thermosciences Division,
Mechanical Engineering Department,
Stanford University,
California 94305-3030
e-mail: sanjiv@stanfordalumni.org

E. Pop

R. W. Dutton

Electrical Engineering Department,
Stanford University,
California 94305-3030

K. E. Goodson
Thermosciences Division,
Mechanical Engineering Department,
Stanford University,
California 94305-3030

Intense electron-phonon scattering near the peak electric field in a semiconductor device results in nanometer-scale phonon hotspots. Past studies have argued that ballistic phonon transport near such hotspots serves to restrict heat conduction. We reexamine this assertion by developing a new phonon transport model. In a departure from previous studies, we treat isotropic dispersion in all phonon branches and include a phonon emission spectrum from independent Monte Carlo simulations of electron-phonon scattering. We cast the model in terms of a non-equilibrium phonon distribution function and compare predictions from this model with data for ballistic transport in silicon. The solution to the steady-state transport equations for bulk silicon transistors shows that energy stagnation at the hotspot results in an excess equivalent temperature rise of about 13% in a 90 nm *gate-length device. Longitudinal optical phonons with non-zero group velocities dominate transport. We find that the resistance associated with ballistic transport does not overwhelm that from the package unless the peak power density approaches* 50 W/μm^3. *A transient calculation shows negligible phonon accumulation and retardation between successive logic states. This work highlights and reduces the knowledge gaps in the electro-thermal simulation of transistors.* [DOI: 10.1115/1.2194041]

Keywords: devices, heat transfer, modeling, nanoscale, thermophysical

1 Introduction

The question of an anomalous temperature rise due to ballistic phonon transport near the heat source in a transistor remains unresolved despite much recent attention [1–4]. It is well known [5] that localized phonon emission from hot electrons near the drain of a semiconductor device results in a heat source with dimensions on the order of 10 nm. Figure 1 shows a typical heat source in a bulk silicon metal-oxide-semiconductor field-effect transistor (MOSFET). The heat generation contours were obtained from a hydrodynamic simulation of electron transport in a 90 nm gate-length device at a supply voltage, V_{dd}, of 1.2 V (with the gate and the drain terminals biased at 1.2 V, and the source terminal grounded). The peak power density is nearly 5 W/μm^3 at saturation conditions in the device. The spatial localization of this hotspot near the drain is a consequence of the sharp peak in the electric field and the short mean free path for electron-phonon scattering. A solution to the heat diffusion equation for this source would predict the temperature field to vary on a length scale comparable to the phonon mean free path in silicon, which is clearly unphysical. Several sub-continuum treatments of this problem are available in the literature as mentioned above. The common conclusion is that there is a substantial difference between the temperature rise predicted by solving the heat conduction equation and the equivalent temperature rise predicted by solving simplified versions of the phonon Boltzmann transport equation (BTE). However, past work has failed to reach a consensus on the scale of this difference and what it implies for transistors deep in the sub-100 nm regime. This is further compounded by the difficulty in experimentally verifying any of the claimed effects.

We expect the phonon distribution function to be nonlocal [6] near the source, resulting in less heat flow than predicted by the theory of heat diffusion. However, the magnitude of this reduction varies widely depending on the assumptions about the phonon dispersion relationship and the phonon frequencies dominating the heat production. The pioneering work of Lai and Majumdar [1] on concurrent electron and phonon transport employed the hydrodynamic model for electrons and a gray-body two-step energy conservation model for optical and acoustic phonons. A temperature rise of 7 K was calculated for the acoustic phonons in a 0.24 μm gate-length silicon MOSFET dissipating 1 mW per unit micrometer width of the device. Heat generation was assumed to be only through optical phonon emission, and the group velocities of optical phonon modes were assumed to be zero. To the best of our knowledge, this assumption has been retained in all subsequent models. We note that no major sub-continuum effect was observed in this study. However, Chen [7] showed that ballistic heat conduction would decrease thermal conductivity locally in the vicinity of a heated nano-particle when the size of the particle was comparable to the phonon mean free path. Expanding upon this result, Sverdrup et al. [2] considered ballistic transport in a 0.4 μm silicon-on-insulator device. Their model showed the lattice temperature rise to be 160% higher than that obtained using the heat diffusion equation. This work assumed a two-fluid dispersion for phonons. More recent efforts [3] extended the energy-moment formulation to account for phonon polarization in the acoustic modes and include frequency-dependent relaxation rates. While the above results were based on energy-moment formulations of the phonon BTE, a recent study [4] used the ballistic-diffusive equations (BDE) to also show this extra temperature rise at the source.

Interestingly, none of the silicon MOSFETs with gate lengths less than 100 nm reported in the literature (see, for example, Ref. [8]) demonstrate any anomalous thermal behavior to the best of our knowledge. While self-heating is a standard problem in the silicon-on-insulator devices, there are no indications of any anomalous heat source size effects as far as their current-voltage characteristics are concerned. This brings up several important questions: Does the presence of a sub-continuum source affect the device characteristics at all? Alternately, do device sources really

Contributed by the Heat Transfer Division of ASME for publication in the Journal of Heat Transfer. Manuscript received June 7, 2005; final manuscript received December 21, 2005. Review conducted by C. P. Grigoropoulos. Paper presented at the 2004 ASME International Mechanical Engineering Congress (IMECE2004), November 13–19, 2004, Anaheim, California, USA.

 Copyright © 2006 by ASME

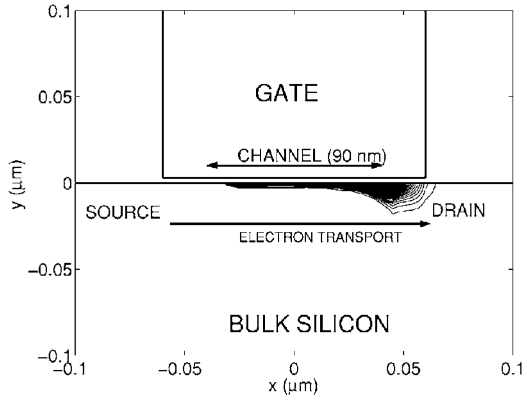

Fig. 1 Contours of heat generation in a 90 nm gate-length bulk silicon *n*-MOSFET are calculated using the hydrodynamic model for electron transport. The peak power density at the center is nearly 5 W/μm^3.

correspond to the sub-continuum sources that microscale heat transfer research has targeted in the past? Are the assumptions used in predicting sub-continuum phonon transport somehow responsible for the reported temperature jumps at the source? Finally, are any of these predictions realistic when it comes to practical devices?

In this paper we attempt to answer the above questions by reformulating the problem and relaxing the assumption of a gray-body heat source. Going beyond this simplification requires details of electron-phonon scattering, which we obtain through Monte Carlo simulations. We solve the phonon BTE for the phonon departure from equilibrium taking into account the simulated electron-phonon scattering term as well as phonon dispersion in the acoustic and optical branches. In our formulation, we split the phonon departure from equilibrium function into two components: one that traces the evolution of the emitted phonons before they thermalize through scattering, and another that traces the diffusion of the thermalized phonons. The former is obtained by solving the ballistic BTE in a spatial region of the order of a mean free path. The latter corresponds to the solution of the BTE in the limit of diffusive transport. We compare the model predictions with existing data on hotspots in a silicon thin film. The solution is extended to predict the temperature field in a bulk silicon device. We make another departure from previous studies by using boundary conditions that take into account the thermal resistance due to the enveloping package. We show that the presence of a hotspot impedes heat conduction locally at the drain in agreement with earlier studies. However, the magnitude is much lower than earlier predictions. Based on this result, we conclude that the emission spectrum in combination with the phonon dispersion ultimately determines the magnitude of the reduced thermal conductance near the hotspot. We argue that the approach of solving either the energy moments of the phonon BTE or the BDE with no consideration of electron-phonon scattering, leads to erroneous conclusions. Finally, we solve the transient problem to investigate phonon accumulation and retardation during switching. This work aims to highlight and close key knowledge gaps in the electro-thermal modeling of sub-100 nm gate-length devices.

2 BTE Formulation for a Phonon Source

We begin the discussion on our model by first reviewing the standard form of the phonon Boltzmann transport equation. This helps us to clarify the reasoning behind our proposed model. Under the relaxation time approximation, the phonon Boltzmann transport equation at steady state is

$$\mathbf{v}_{\mathbf{k},s}\cdot\nabla N_{\mathbf{k},s} = -\frac{N_{\mathbf{k},s}-\bar{N}}{\tau_{\mathbf{k},s}} \tag{1}$$

where $(\mathbf{k},s)$ refers to the phonon mode with wave vector $\mathbf{k}$ and polarization s, $\mathbf{v}$ is the group velocity, N is the phonon occupation number, $\bar{N}$ is the equilibrium Bose-Einstein distribution function, τ is the net relaxation time from all scattering events. A common approach to solve the BTE is to write the distribution function as a departure from equilibrium function, η, added to the Bose-Einstein equilibrium distribution function

$$N = \bar{N}(T) + \eta_{\mathbf{k},s} \tag{2}$$

Substitution in the BTE yields an explicit solution for $\eta_{\mathbf{k},s}$ under the assumption that terms of second order in the temperature gradient and the term involving the gradient in the departure function are much smaller than the other terms, and may be neglected. The departure from equilibrium function thus obtained is proportional to the temperature gradient and conforms to the Fourier heat flux law

$$\eta_{\mathbf{k},s} = -\tau_{\mathbf{k},s}\mathbf{v}_{\mathbf{k},s}\cdot\nabla T\frac{\partial\bar{N}}{\partial T} \tag{3}$$

The above first order approximation works well provided the temperature gradient is small enough that the change in temperature over the relaxation length is much smaller than the absolute value of the temperature [9]. That is

$$\frac{\partial T}{\partial x}v\tau \ll T \tag{4}$$

a condition that is usually valid. However, when the second order derivative of T varies on a length scale comparable to the mean free path, the heat flux is nonlocal in the phonon distribution function. Claro and Mahan [6,10] showed that this leads to much higher temperature gradients than those predicted by the Fourier law of heat conduction.

We expect a confined high density source of phonons such as a device hot spot to also show non-local effects. In this case the nonlocality arises not due to higher order temperature derivatives but due to the gradient in the departure function itself. The departure from equilibrium function will be essentially dictated to first order by the distribution of emitted phonons in the real and reciprocal spaces of the crystal. Thus, large spatial gradients in the source function that arise when the hotspot is small compared to the phonon mean free path, translate to large gradients in the departure function as well, that is

$$\frac{\partial\eta^*_{\mathbf{k},s}}{\partial x^*} \sim \dot{n}^*_{\mathbf{k},s}\tau_{\mathbf{k},s} \tag{5}$$

to first order where the $\dot{n}_{\mathbf{k},s}$ is the net phonon emission from electron-phonon scattering. The asterisk in the superscript indicates a normalized quantity, with the mean free path and the equilibrium distribution function chosen as the appropriate scaling factors. The term on the right is large provided the electron-phonon relaxation rate is greater than the phonon-phonon relaxation rate. The disparity in the electron and phonon energy relaxation rates is estimated to be about two orders of magnitude in a submicrometer MOSFET operating at room temperature. The relaxation rate is about 10^{13} s^{-1} for electrons and about 10^{11} s^{-1} for optical phonons [11,12] in silicon. Thus, the gradient in the departure from equilibrium function cannot be neglected in the case of electro-thermal transport in transistors as it is in the formulation for thermal conductivity.

We modify the formulation by first including a source term in the phonon BTE that provides the net phonon emission rate due to electron scattering. The actual source function is obtained through detailed Monte Carlo simulations as described later. Other phonon scattering events are modeled through the relaxation time approxi-

mation and a reciprocal sum of the relaxation times is taken to represent the overall relaxation rate of a mode. The expressions for the relaxation times can be obtained from first order perturbation theory and empirical fits have been developed by Holland [13]. Thus, the steady-state evolution can be written as

$$\mathbf{v}_{\mathbf{k},s} \cdot \nabla N_{\mathbf{k},s} = -\frac{N_{\mathbf{k},s} - \bar{N}}{\tau_{\mathbf{k},s}} + \dot{n}_{\mathbf{k},s} \tag{6}$$

where $\dot{n}$ is the phonon emission. Proceeding as in the formulation for thermal conductivity, we write N as a small perturbation, η, over the equilibrium distribution function as given in Eq. (2). The BTE, written in terms of $\eta_{\mathbf{k},s}$, is

$$\mathbf{v}_{\mathbf{k},s} \cdot \left(\nabla \eta + \nabla T \frac{\partial \bar{N}}{\partial T} \right) = -\frac{\eta_{\mathbf{k},s}}{\tau_{\mathbf{k},s}} + \dot{n}_{\mathbf{k},s} \tag{7}$$

To obtain a solution to the non-homogeneous BTE, we first subtract the near-equilibrium departure function as given by Eq. (3) from $\eta_{\mathbf{k},s}$. The remainder is the far-from-equilibrium departure function that is due to the phonon emission source term. Thus,

$$\eta_{\mathbf{k},s} = -\tau_{\mathbf{k},s} \mathbf{v}_{\mathbf{k},s} \cdot \nabla T \frac{\partial \bar{N}}{\partial T} + n_{\mathbf{k},s} \tag{8}$$

where $n_{\mathbf{k},s}$ is the far-from-equilibrium departure function. The idea behind Eq. (8) is that the phonon flux at any point in space is due to a near-equilibrium part that obeys the Fourier law superposed on a second contribution due to the emission spectrum that does not obey the Fourier law. As we move farther away from the hotspot, we expect the second contribution to diminish strongly as the emitted phonons thermalize, and the Fourier law contribution to increase proportionately to maintain energy continuity. The BTE thus becomes

$$\mathbf{v}_{\mathbf{k},s} \cdot \left[\nabla n_{\mathbf{k},s} - \nabla \left(\tau_{\mathbf{k},s} \mathbf{v}_{\mathbf{k},s} \cdot \nabla T \frac{\partial \bar{N}}{\partial T} \right) \right] = -\frac{n_{\mathbf{k},s}}{\tau_{\mathbf{k},s}} + \dot{n}_{\mathbf{k},s} \tag{9}$$

Additionally, macroscopic energy continuity must be satisfied and this is written at steady state as

$$\nabla \cdot \mathbf{J} = \dot{Q} \tag{10}$$

where $\mathbf{J}$ is the heat flux vector and $\dot{Q}$ is the heat generation rate. These are expressed in terms of the non-equilibrium distribution functions as follows

$$\dot{Q} = \sum_s \frac{1}{8\pi^3} \int \dot{n}_{\mathbf{k},s} \hbar \omega_{\mathbf{k},s} d\mathbf{k} \tag{11}$$

$$\mathbf{J} = \sum_s \frac{1}{8\pi^3} \left[\int \mathbf{v}_{\mathbf{k},s} n_{\mathbf{k},s} \hbar \omega_{\mathbf{k},s} d\mathbf{k} - \int \mathbf{v}_{\mathbf{k},s} \tau_{\mathbf{k},s} \mathbf{v}_{\mathbf{k},s} \cdot \nabla T \frac{\partial \bar{N}}{\partial T} \hbar \omega_{\mathbf{k},s} d\mathbf{k} \right] \tag{12}$$

where the integration is taken over the first Brillouin zone. The second term in the heat flux vector can be written in terms of the thermal conductivity tensor, $\mathbf{K}$, so that Eq. (12) reduces to

$$\mathbf{J} = \sum_s \frac{1}{8\pi^3} \int \mathbf{v}_{\mathbf{k},s} n_{\mathbf{k},s} \hbar\, \omega_{\mathbf{k},s} d\mathbf{k} - \mathbf{K} \cdot \nabla T \tag{13}$$

With the above expression for the heat flux vector, Eq. (10) can be integrated to give

$$\sum_s \frac{1}{8\pi^3} \int \mathbf{v}_{\mathbf{k},s} n_{\mathbf{k},s} \hbar \omega_{\mathbf{k},s} d\mathbf{k} - \mathbf{K} \cdot \nabla T = \int \dot{Q} d\mathbf{r} \tag{14}$$

Equations (9) and (14) form a closed system with the unknowns being $n_{\mathbf{k},s}$ and T.

However, this system is still difficult to solve without further simplification. We note that the second term on the left in Eq. (9) is a second order term in the temperature gradient and can be neglected. This approximation causes the temperature field to be independent of the emitted phonons until they thermalize through scattering. The field does influence the far-from-equilibrium distribution indirectly through the temperature dependence of the phonon scattering rates. With the above approximation, the BTE is of the form

$$\mathbf{v}_{\mathbf{k},s} \cdot \nabla n_{\mathbf{k},s} = -\frac{n_{\mathbf{k},s}}{\tau_{\mathbf{k},s}} + \dot{n}_{\mathbf{k},s} \tag{15}$$

To solve the system we need to specify the boundary conditions. We take this up in the following sections when we develop analytical solutions for specific cases. Knowing the distribution function $n_{\mathbf{k},s}$ the continuity of energy must be solved for the temperature field.

Proceeding as above, we can also derive time dependent equations. Assuming that the temporal variation in temperature is much slower than that in the departure function, we can drop the transient temperature term in the BTE. The transient form is thus

$$\frac{\partial n_{\mathbf{k},s}}{\partial t} + \mathbf{v}_{\mathbf{k},s} \cdot \nabla n_{\mathbf{k},s} = -\frac{n_{\mathbf{k},s}}{\tau_{\mathbf{k},s}} + \dot{n}_{\mathbf{k},s}(t) \tag{16}$$

The time dependent energy conservation equation is

$$C\frac{\partial T}{\partial t} + \frac{\partial}{\partial t}\left(\sum_s \frac{1}{8\pi^3} \int n_{\mathbf{k},s}\, \hbar\, \omega_{\mathbf{k},s} d\mathbf{k} \right) = \dot{Q} - \nabla \cdot \left[\sum_s \frac{1}{8\pi^3} \int \mathbf{v}_{\mathbf{k},s} n_{\mathbf{k},s} \hbar \omega_{\mathbf{k},s} d\mathbf{k} - \mathbf{K} \cdot \nabla T \right] \tag{17}$$

where C is the lattice heat capacity.

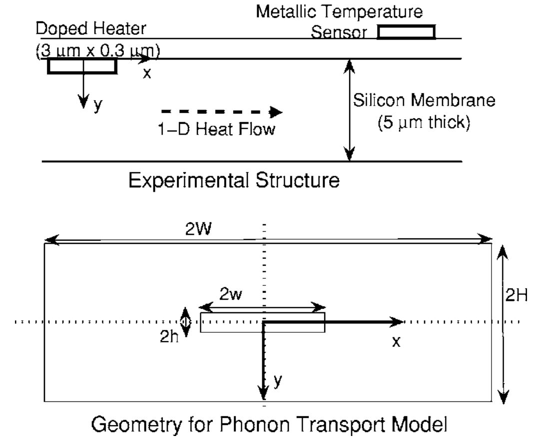

Fig. 2 A cross section of the experimental structure used to probe ballistic conduction near a doped resistor in silicon [14] is shown at the top. The resistor acted as a hotspot inside the silicon membrane. The symmetry in the problem is used to solve the BTE in the domain shown below.

3 Comparison With Data for Ballistic Transport

In this section we use the above model to predict the thermal resistance associated with ballistic transport near a hotspot in silicon. Sverdrup et al. [14] used heating in a doped resistor thermometer in silicon to create a micrometer scale phonon source in a membrane structure, shown schematically in Fig. 2. In this experiment, a 3-μm-wide region in a 5-μm-thick n-type silicon membrane was p doped to a depth of about 0.3 μm. A bias applied across the terminals of the resistor forced a current through the doped region. By reverse biasing the p-n junction between the resistor and the substrate, the current was confined within the doped region. Joule heating in the doped resistor induced a temperature rise in the membrane structure. The thermal resistance of

the silicon membrane was determined from the temperature rise detected by the metallic sensors, placed parallel to the doped resistor, and by the resistor itself. The experiment was conducted in the ambient temperature range of about 100–300 K. The thermal resistance showed a large deviation from the predictions of the Fourier law at low temperatures indicating non-diffusive behavior close to the resistor.

We now calculate the thermal resistance measured in the experiment using our model. The problem is much simplified by considering the symmetry of the source and the boundary conditions. We expect scattering at the membrane boundary to be largely diffuse in the temperature range of the experiment since the phonon wavelength is comparable to the surface roughness. Thus, the BTE of Eq. (15) may be solved in the domain shown at the bottom of Fig. 2 with homogeneous boundary conditions at all four boundaries. The two-dimensional BTE in rectangular coordinates is

$$v_x \frac{\partial n_{\mathbf{k},s}}{\partial x} + v_y \frac{\partial n_{\mathbf{k},s}}{\partial y} = -\frac{n_{\mathbf{k},s}}{\tau_{\mathbf{k},s}} + \dot{n}_{\mathbf{k},s} \tag{18}$$

We solve the above wave equation by the method of characteristics and get the solution in velocity space as follows

$V_x < 0$	$V_x > 0$
$(2W-x) < -y\frac{v_x}{v_y}: G(x,y)$	$x < y\frac{v_x}{v_y}: G(x,y)$
$(2W-x) > -y\frac{v_x}{v_y}: F(x,y)$	$x > y\frac{v_x}{v_y}: F(x,y)$
$(2W-x) < -(2H-y)\frac{v_x}{v_y}: G(x,y)$	$x < -(2H-y)\frac{v_x}{v_y}: G(x,y)$
$(2W-x) > -(2H-y)\frac{v_x}{v_y}: F(x,y)$	$x > -(2H-y)\frac{v_x}{v_y}: F(x,y)$

(Upper rows: $V_y > 0$; lower rows: $V_y < 0$.)

where the functions F and G are defined as

$$F(x,y) \equiv \int_0^y \frac{\dot{n}(x,y')}{v_y} \tau e^{\frac{y'-y}{\tau v_y}} dy'$$

$$G(x,y) \equiv \int_0^x \frac{\dot{n}(x',y)}{v_y} \tau e^{\frac{x'-x}{\tau v_x}} dx' \tag{19}$$

Since the resistor was p doped, phonon emission in the experiment was from hole-phonon scattering. Unfortunately, the emission spectrum for holes at the electric fields employed in the experiment is not available in the literature. In the absence of any spectral information about the emitted phonons, we proceed by integrating the departure function over frequency to get the net power density which is known from the experiment. The net thermal resistance at the source is the sum of the diffusion and BTE resistances. Thus

$$R = R_{\text{diffusion}} + R_{\text{BTE}}$$

$$\text{with } R_{\text{diffusion}} = \frac{1}{\pi K_M}\left[\frac{\pi W}{2H} + ln\left(\frac{H}{2h+w}\right)\right] \tag{20}$$

where w and h are the cross-sectional width and height, respectively, of the doped resistor, H is the thickness of the membrane, W is half the width of the membrane, K_M is the thermal conductivity in the membrane. Details regarding derivation of the two-dimensional thermal resistance from diffusion theory may be found in Hahne and Grigull [15].

The BTE resistance of Eq. (20) is a hypothetical resistance and is a measure of the difference between the diffusion temperature and the equivalent temperature calculated from the BTE model. We define the equivalent temperature, T_{EQ}, similar to previous work [1,7,16] on non-equilibrium phonon transport

$$\frac{1}{8\pi^3}\sum_s \int \bar{N}(T_{EQ})\hbar\omega d\mathbf{k} = \frac{1}{8\pi^3}\sum_s \int \bar{N}(T)\hbar\omega d\mathbf{k} + \frac{1}{8\pi^3}\sum_s \int n\hbar\omega d\mathbf{k} \tag{21}$$

We note that the first term on the right in Eq. (8), which is proportional to the temperature gradient, does not contribute to the energy integral. With the above definition we can represent the nonequilibrium among the modes in terms of the equivalent temperature.

In order to obtain R_{BTE} we rewrite Eq. (21) in terms of the lattice heat capacity, C, and estimate the difference in the peak lattice and equivalent temperatures. The integration over phonon frequencies is simplified by assuming phonons near the source to have a mean free path Λ and a mean relaxation time τ. Using the velocity space solution given above

$$C(T_{EQ} - T_{\text{ref}}) = C(T - T_{\text{ref}}) + \frac{1}{4\pi}\int \dot{n}\tau\hbar\omega g(\omega)d\omega \times 4\left[\int_{\mu>\frac{W}{H}\eta}\int_{\eta>0}\frac{d\mu d\eta}{\sqrt{1-\mu^2-\eta^2}}(1-e^{-\frac{h}{\mu\Lambda}}) + \int_{\eta>\frac{H}{W}\mu}\int_{\mu>0}\frac{d\mu d\eta}{\sqrt{1-\mu^2-\eta^2}}(1-e^{-\frac{w}{\eta\Lambda}})\right]$$

$$\text{or, } (T_{EQ} - T)|_{x=0} = \frac{1}{C}\int \dot{n}\tau\hbar\omega g(\omega)d\omega \times f(w,h,\Lambda) = \frac{\dot{Q}_{max}\tau_s}{C} f(w,h,W,H,\Lambda) \tag{22}$$

where μ, η are the direction cosines along x and y, respectively, Λ is the phonon mean free path, and $\dot{Q}_{\max}$ is the peak heat generation rate, at x=0. The heat generated in the diode is fairly uniform across its cross section and we may use the average power instead of $\dot{Q}_{\max}$. The effective scattering time τ_s is given by the ratio of the summation of $\dot{n}\tau$ over all modes to the peak generation rate and is a fitting parameter in this calculation since the function $\dot{n}$ is unknown. The thermal resistance sustaining the peak difference between T_{EQ} and T is

$$R_{\text{BTE}} = \frac{(T_{EQ} - T)|_{x=0}}{q} = \frac{\dot{Q}_{\max}\tau_s}{qC} f(w,h,W,H,\Lambda) \tag{23}$$

where q is the total heat current flowing to the sink. The geometry factor f is unity at room temperature, where $w,h \gg \Lambda$, and decreases slightly with temperature as the mean free path increases in relation to the source dimensions.

The dominant effect of the decreasing temperature is to increase R_{BTE}. The net increase is, in turn, due to the decrease in the heat capacity and the increase in the effective scattering time of emitted phonons. This is shown in Fig. 3 which compares the thermal resistance measured by the doped resistor at different base temperatures with predictions based on Eqs. (20) and (23). We note that in the absence of information about the emission spectrum, we have fit the model using a *constant* value for the effective scattering time for emitted phonons, τ_s, which is on the order of 10 ns. This represents a weighted average of the scattering times of all emitted phonons, the weights being the relative excitation numbers of different modes. A better fit could be obtained in principle if we include a temperature dependence of the mean scattering time. However, this is quite complicated in practice because it

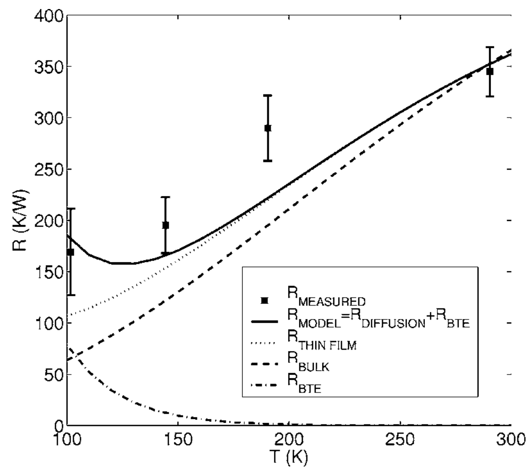

Fig. 3 A comparison of the thermal resistance measured at different temperatures. Predictions based on the proposed model are given by the continuous line. The predictions suffer from lack of information on temperature dependent scattering rates of phonons emitted by holes in silicon.

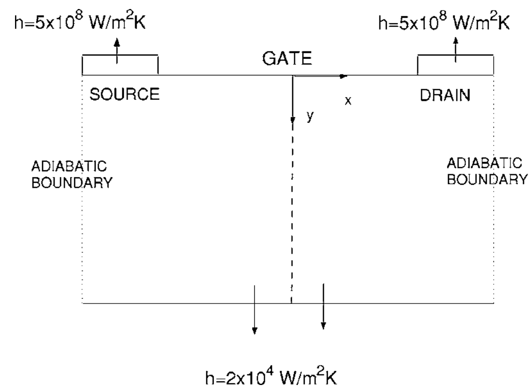

Fig. 4 The boundary conditions used in the device calculations are shown above. Heat is assumed to flow out through the metallic contacts at the top which act as fins. The heat transfer coefficient is relatively high due to this spreading effect. Most of the heat flow is toward the heat sink through the bulk silicon at the bottom.

involves the temperature dependence of not just the phonon relaxation times but also that of the weights. The latter would require detailed Monte Carlo simulations of hole-phonon scattering at each base temperature. Hence, we omit any temperature dependence of the mean scattering time in the absence of a clear intuition about the temperature dependence of the weights. The dashed line shows the thermal resistance of the membrane structure calculated from diffusion theory using the bulk thermal conductivity of silicon. Phonon boundary scattering reduces the thermal conductivity of the membrane so that the bulk predictions are significantly lower than the data. The dotted line is the thermal resistance calculated from diffusion theory (Eq. (20)) but using the thermal conductivity of the membrane measured in situ. The measurements increasingly differ from predictions of diffusion theory as the temperature decreases. We attribute this to ballistic phonon transport near the doped resistor. Phonons emitted at the heat source increasingly undergo boundary scattering as the ambient temperature decreases. This leads to a temperature slip at the heat source and causes the temperature rise to deviate from heat diffusion theory. The solid line represents the sum total of the BTE and diffusion resistances. The predictions from Eq. (20) agree well with the data at 100 and 140 K, where the departure from diffusion theory is substantial. The model is, however, unable to match the data at 190 K. Additionally, the trend curve for the data appears to have an inflection point between 140 and 190 K. The sub-continuum contribution appears to asymptote at low temperatures, whereas the model predicts ever-increasing contributions due to increasing mean free paths. We speculate that this deviation from the model may be due to the mean free path in the thin film becoming constrained by boundary scattering at low temperatures. We note that a mean free path based on the thin-film thermal conductivity and calculated from the simple kinetic theory expression of $\Lambda=3\ K/Cv$ would not reproduce this trend. Thus, although the qualitative behavior of the trend in the data is understandable, we are unable to obtain a good quantitative match, primarily due to lack of information about the temperature dependence of the mean scattering time for reasons discussed above.

4 Application to a Bulk Silicon MOSFET

In this section we use our model to compute the phonon distribution function in a 90 nm gate-length bulk silicon *n*-type MOSFET (NMOS). We specifically choose an NMOS device because its higher power density would increase the magnitude of any sub-continuum effects. As shown in Fig. 1, the hot spot predicted by a hydrodynamic calculation is formed in the channel under the gate toward the drain side. We note that device Monte Carlo simulations, however, predict the location to be shifted more toward the drain. The precise location is unimportant in this work since the boundaries for the thermal calculation are much larger in extent when compared to this shift in the location of the hot spot. We are more interested in the shape of the hot spot, which is predicted reasonably well by hydrodynamic calculations. The shape is approximately semicylindrical in a bulk MOSFET, with the axis aligned along the width of the device. In order to proceed toward a semi-analytical solution to our model, we approximate the location of the source to be midway between the source and the drain. As noted above, this shift in location is much smaller than the lateral extent of the device. Hence, we do not expect a major difference in our results due to this approximation. Figure 4 shows the device with the approximated source at the origin. The top boundary is assumed to be adiabatic due to the insulating gate oxide. In reality, there is a small heat flux across this interface which is ignored in our calculations to simplify the BTE solution. The side boundaries are both adiabatic due to thick isolation oxides. Some heat is lost through the metallic contacts as shown. We obtain the heat transfer coefficients by treating the metallic interconnects as fins [17]. The heat produced in the transistor mostly flows out at the bottom toward the heat sink, after passing through the bulk silicon. We assume the power density at the source to be $5\ \mathrm{W}/\mu\mathrm{m}^3$, scaled down by an activity factor of 0.1 (to account for average circuit activity), and the radius to be 20 nm which closely approximate realistic device hotspots. The device hot spot is further assumed to be a step function as shown in Fig. 5. The phonon spectrum in the heat production region is obtained through a Monte Carlo simulation as described below.

4.1 Electron-Phonon Scattering Using the Monte Carlo Method. The purpose behind formulating our BTE model in terms of the non-equilibrium phonon distribution function, as opposed to some fictitious temperature, is to solve it with a frequency-dependent source term without invoking questionable arguments about equivalent temperatures. Before we can solve the simplified phonon BTE, however, we need the source term, $\dot{n}_{\mathbf{k},s}$, appearing in Eq. (15). Ideally, the source term should couple the conservation of energy equations for electrons and phonons. In this work, we avoid that considerable complication by decoupling electron and phonon transports. In effect, we assume electron-phonon scattering to proceed between non-equilibrium electrons and equilibrium phonons. We employ Monte Carlo simulations of electron-phonon scattering to extract phonon emission rates in

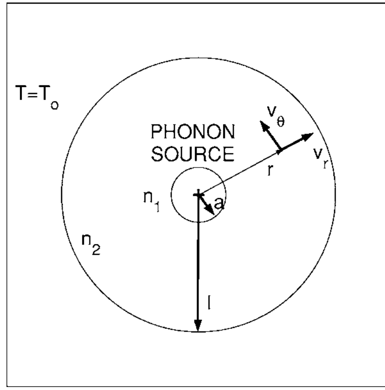

Fig. 5 The cylindrical geometry resulting from the assumption that the hotspot is located at the center of the channel serves to reduce the complexity. We further assume a step profile with the heat source confined to a radius a, as shown schematically.

silicon at a constant electric field. Details of this work are provided separately in Refs. [18,19] and are beyond the scope of this paper. We include a brief overview here for the reader's convenience.

Our Monte Carlo approach employs analytic approximations for the electron energy bands and the phonon dispersion. This band approximation for electrons is reasonable for device voltages near or below the silicon band gap (1.1 eV), such as those of future nano-technologies, and it represents an efficient implementation of the otherwise time-consuming Monte Carlo approach. The simulation treats all phonon scattering events as inelastic. Electrons exchange energy with the lattice as determined by the phonon dispersion and scattering selection rules. Scattering with intravalley longitudinal acoustic (LA) and transverse acoustic (TA) phonons, as well as with intervalley longitudinal optical (LO) and transverse optical (TO) phonons, is considered individually. The phonon dispersion relationship is used to compute the final electronic state in a manner that conserves both momentum and energy. During the simulation all phonons absorbed and emitted are tallied and net phonon emission statistics can be computed. Figure 6 shows the analytic (quadratic) phonon dispersion used in this work and the computed phonon emission spectrum at a field of 4 MV/m. To facilitate comparison the vertical axes are drawn with the same energy units. The peaks in the phonon generation rate occur due to selection rules for the electron-phonon interaction. The relative magnitude of the peaks depends on the choice of scattering deformation potentials, which are calibrated across a wide temperature range [18]. In terms of energy, LO emissions make up about half, LA emissions about a third and TO emissions about a tenth of the heat generation rate in bulk silicon at typical electric fields. In the next section, we use the emission rate to compute steady-state phonon occupations for individual phonon frequencies.

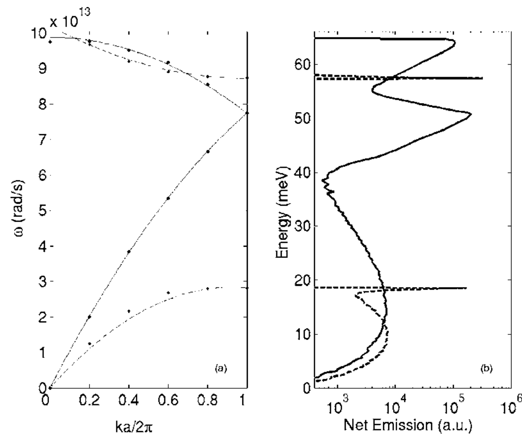

Fig. 6 The phonon dispersion in silicon along [100] is obtained from a fit to neutron scattering data from Dolling [23]. The above dispersion is assumed to hold along all directions in our calculations. At an electric field of 4 MV/m, the source term in the BTE, $\dot{n}_{\mathbf{k},s}$, has the frequency dependence shown on the right.

4.2 Analytical Solution to the Phonon BTE. The two-dimensional BTE for the device problem is as given in Eq. (18). By approximating the source to be a semicylinder located at the origin, we can take advantage of the resulting radial symmetry. We convert Eq. (18) to radial coordinates as follows

$$v_r \frac{\partial n_{\mathbf{k},s}}{\partial r} + \frac{v_\theta^2}{r}\frac{\partial n_{\mathbf{k},s}}{\partial v_r} - \frac{v_\theta v_r}{r}\frac{\partial n_{\mathbf{k},s}}{\partial v_\theta} + \frac{n_{\mathbf{k},s}}{\tau_{\mathbf{k},s}} = \dot{n}_{\mathbf{k},s} \tag{24}$$

where v_r and v_θ are the radial and tangential velocities as depicted in Fig. 5. Due to axial symmetry, there is no dependence on the azimuthal angle, θ. To obtain an analytic solution we split the solution into two domains, subscripted with indices 1 and 2 as shown schematically in Fig. 5. For $r \leqslant a$, where a is the radius within which the source is confined, the BTE is nonhomogeneous, whereas for $r > a$ the equation is homogeneous

$$v_r \frac{\partial n_1}{\partial r} + \frac{v_\theta^2}{r}\frac{\partial n_1}{\partial v_r} - \frac{v_\theta v_r}{r}\frac{\partial n_1}{\partial v_\theta} + \frac{n_1}{\tau} = \dot{n}$$

$$v_r \frac{\partial n_2}{\partial r} + \frac{v_\theta^2}{r}\frac{\partial n_2}{\partial v_r} - \frac{v_\theta v_r}{r}\frac{\partial n_2}{\partial v_\theta} + \frac{n_2}{\tau} = 0 \tag{25}$$

The solution to Eq. (25) can be obtained by reducing the system to a form that corresponds to the BTE for electron transport in a metallic wire [20] for which the general solution is known. We find the general solution to Eq. (25) to be

$$n_1 = \dot{n}\tau\left[1 - \exp\left(-\frac{r v_r}{\tau(v_r^2 + v_\theta^2)}\right) f_1(r v_\theta, v_r^2 + v_\theta^2)\right]$$

$$n_2 = \dot{n}\tau \exp\left(-\frac{r v_r}{\tau(v_r^2 + v_\theta^2)}\right) f_2(r v_\theta, v_r^2 + v_\theta^2) \tag{26}$$

where f_1 and f_2 are arbitrary functions to be determined from boundary conditions. The boundary conditions for the problem are

$$n_2(r = l, -|v_r|, v_\theta) = 0$$

$$n_1(r = 0, |v_r|, v_\theta) = n_1(r = 0, -|v_r|, v_\theta)$$

$$n_1(r = a, \pm|v_r|, v_\theta) = n_2(r = a, \pm|v_r|, v_\theta) \tag{27}$$

Applying the boundary conditions, the final solution is

$$n_1 = \dot{n}\tau\left[1 - \exp\left(\frac{-r v_r + \sqrt{a^2(v_r^2 + v_\theta^2) - r^2 v_\theta^2}}{\tau(v_r^2 + v_\theta^2)}\right)\right]$$

$$n_2(v_r > 0) = 2\dot{n}\tau \exp\left(-\frac{r v_r}{\tau(v_r^2 + v_\theta^2)}\right) \times \sinh\left(\frac{\sqrt{a^2(v_r^2 + v_\theta^2) - r^2 v_\theta^2}}{\tau(v_r^2 + v_\theta^2)}\right)$$

$$n_2(v_r < 0) = 0 \tag{28}$$

In order to evaluate the above expressions, we need the phonon relaxation times. For the relaxation times of the acoustic modes, we use the expressions developed by Holland [13] and fit to thermal conductivity data for bulk silicon. We use a single value of 10 ps for all optical modes which is on the order of the room temperature lifetime of zone-center optical modes in silicon measured by Raman spectroscopy [12]. We now compare the model predictions with a numerical solution to the heat diffusion equa-

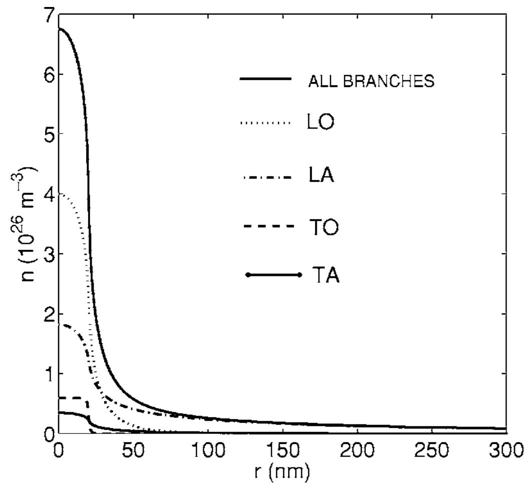

Fig. 7 The phonon number density for different branches is shown close to the hotspot, which is 20 nm in extent. The LO contribution dominates the number density and consequently, the energy density.

tion in a 90 nm gate length device.

It is interesting to compare the non-equilibrium contribution of the different phonon branches to the number density and the non-Fourier heat flux. Due to strong emission in the LO modes, the LO contribution is more than 50% of the total non-equilibrium number density. Figure 7 shows the contribution from all four branches near the hotspot. The energy density is also proportionately higher for the LO branches since LO frequencies are higher compared to other branches. The LO and the LA branches are dominant contributors to heat conduction. This is evident from Fig. 8 where the contributions of individual branches to the heat flux are plotted. We note that the flux is zero for all branches at $r=0$ due to the imposed symmetry condition. The contributions of TA and TO are insignificant. The non-Fourier heat flux diminishes rapidly outside the hotspot, as expected from the ballistic nature of the equations. At the point where it peaks, the non-Fourier heat flux is still only 5% of the total heat flux. Therefore, heat conduction is dominated by the Fourier contribution according to this model.

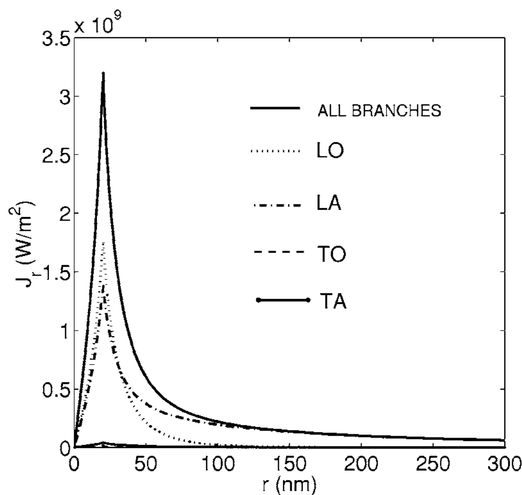

Fig. 8 The non-Fourier heat flux due to different phonon branches is shown. Ballistic heat conduction is predominantly through LO phonons. The cumulative flux is only about 5% of the total, the rest being the flux due to thermalized phonons that obey the Fourier law.

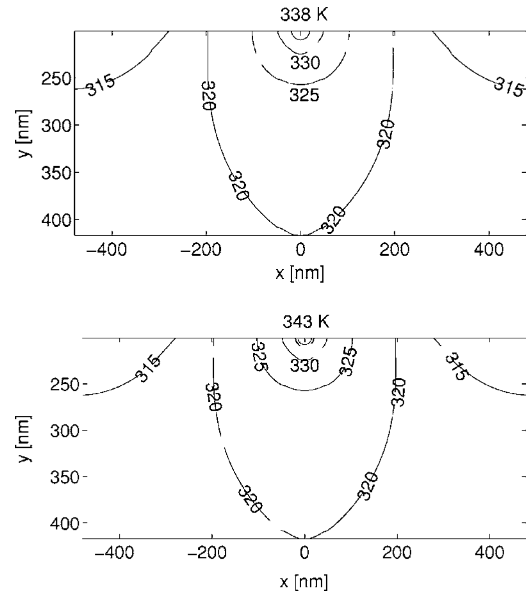

Fig. 9 A comparison of the temperature fields obtained from continuum heat diffusion and phonon heat conduction is shown above. Ballistic conduction augments the overall thermal resistance between the transistor and the ambient by about 13%.

The impact of the non-local departure from equilibrium is, however, quite strong near the hotspot in terms of the local energy density, which is characterized by the equivalent temperature of Eq. (21). Figure 9 compares the temperature field in the device obtained from the heat diffusion equation with that from the proposed model. The BTE model predicts an excess temperature rise of 5 K, above the peak temperature rise of about 38 K from heat diffusion. The LO branch is "hotter" than the acoustic branches, with the branch temperature being 358 K. We note that these magnitudes are very sensitive to boundary conditions. Based on these numbers, the peak equivalent lattice temperature rise is nearly 13% more than the peak temperature rise computed assuming heat diffusion for a 90 nm device. Most of the excess energy is resident in longitudinal optical phonons. The equivalent temperature rise for LO modes alone is 37% higher than that for the entire phonon ensemble, and is a measure of the nonequilibrium among phonons.

We now examine the implications of the above results in the context of the questions posed at the beginning. We emphasize that the major departure in the present treatment comes from handling of the heat source term in the phonon BTE and from solving directly for phonon distribution functions instead of hypothetical equivalent temperatures. The second aspect is critical because it altogether avoids attaching hypothetical equivalent temperatures to phonon branches as well as defining energy exchange between branches. We feel that the latter approach is arbitrary because energy mixing between phonon modes does not proceed strictly on the basis of polarization. Polarization merely decides the symmetry for selection rules in most cases. The first thing to note in the above results is the preponderance of LO phonons, not just in terms of the energy density but also in terms of the heat flux. Earlier studies have repeatedly assumed optical phonons to possess zero group velocities based on the usual flatness of their dispersion relation. We note that in reality the g-LO phonon, that is most likely to scatter with electrons, possesses a group velocity of about 1500 m/s. This is reflected in our results in terms of the dominating LO contribution to the heat flux. Further, by including boundary conditions that take into account thermal resistances all the way up to the package, we are able to gauge the importance of

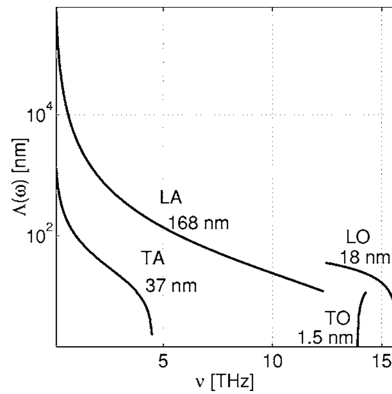

Fig. 10 The distribution of free paths in room temperature silicon as a function of phonon frequency and polarization is shown. The mean free path of phonons emitted by hot electrons in a device are also given for comparison. The use of a gray-body approximation for the heat source would lead to significant errors in predictiing the ballistic nature of transport near hotspots.

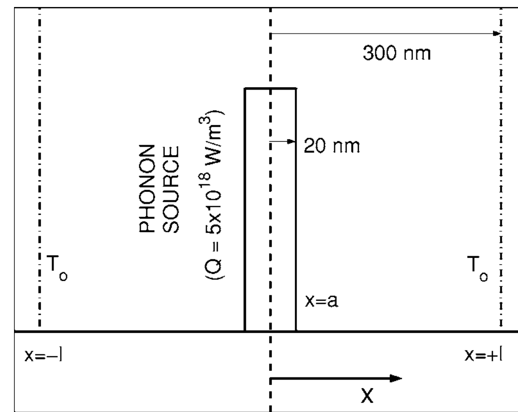

Fig. 11 A step-like phonon source symmetric about *x*=0 with a uniform power density of 5 W/μm^3 is considered for a sample transient calculation. The extent of the source, *a*, is taken to be 20 nm, consistent with device hotspots. A sink at 300 K is assumed to be present at *x*=±*l* where *l*=300 nm.

sub-continuum resistance in relation to that of the continuum junction to ambient resistance. While ballistic transport serves to create hotspots more intense than predicted otherwise by diffusion theory, the chip package remains the dominant thermal resistance. Thus, our results do not suggest the source-size effect to lead to device reliability issues in bulk devices at current electric field levels. If, however, the peak electric field and the current density increase in future devices so as to augment the peak volumetric power density by an order to magnitude (to about 50 W/μm^3), then the resultant phonon density at the hotspot would lead to reliability concerns in the drain. In this case, we estimate that sub-continuum effects would increase the thermal resistance by about 30–40%. An important aspect not considered thus far is the implication of sub-continuum effects on leakage currents. The drain to substrate junction is an important source of leakage currents. High phonon densities in the drain could promote leakage currents by increasing the thermal energy of the electrons. To the best of our knowledge, this consideration is not available in the literature. We caution that the use of equivalent temperatures obtained from BTE calculations in the usual empirical relation between leakage currents and temperature (see [21], for example) would lead to unreasonable predictions since such relations are derived on the assumption of thermodynamic equilibrium.

Finally, we examine the often-used concept of a phonon mean free path in the context of transport in silicon transistors. Generally, a phonon mean free path on the order of 100 nm is used for gray-body calculations. However, from our consideration of electron-phonon scattering and subsequent phonon transport, we find that the above figure derived from consideration of thermal conductivity of silicon is misleading, when it comes to transport near hotspots in transistors. As pointed out above, transport in the vicinity of the hotspot is far from equilibrium and has little to do with thermal conductivity of the medium. The mean free path of phonons emitted at the hot spot depends strongly on the phonon emission spectrum. Figure 10 shows the free paths of phonons in silicon as a function of frequency and polarization at 300 K based on the Holland model [13] for thermal conductivity. Also shown are the mean free paths of phonons in the emission spectrum for different branches. As evident from the figure, the phonons dominating the emission spectrum (the LO phonons) have a mean free path of about 15 nm, much smaller than the commonly used figure of 100 nm.

We explain the origin of the large deviations from heat diffusion theory reported in previous studies as follows. Essentially, none of these studies describe a pure source-size effect. The choice of a large mean free path based on a thermal phonon distribution and the selection of a thin film geometry (silicon-on-insulator device) leads to the termination of the hot phonon free paths at the film boundary. This gives rise to a large temperature slip at the heat source in the same manner as in the low temperature experiment discussed previously. *The size of the source is not the primary factor* but rather the thickness of the film in relation to the mean free path used in the study. The choice of a zero group velocity for optical phonons serves to increase the magnitude of the slip. Based on our calculations above, the phonon distribution at the heat source corresponds to a smaller mean free path. Additionally, the optical contribution corresponds to a non-zero group velocity. Thus, we do not expect the heat sources in real devices operating at room temperature to demonstrate a temperature slip unless the device is built on ultrathin film silicon with thickness down to 15 nm. This estimate of the thickness is based on the assumption that the peak electric field remains similar to that considered here. However, for a slip to occur phonons must be emitted in the direction of the thin-film boundaries. Since quantum confinement of electrons in an ultrathin film silicon channel leads to the heat source migrating away from the gate oxide interface to the middle of the channel, it is difficult to predict if the conditions required for the temperature slip would be exactly satisfied in this geometry.

5 Transient Phonon Distributions During Switching

Although the above analysis considered a steady-state phonon source, in reality, the source is time dependent if the transistor is operating in a circuit. A transistor in a digital circuit typically switches on a time scale of about 100 ps. Ignoring leakage power, a complementary metal-oxide-semiconductor device dissipates power over only a fraction of this period, referred to as the duty cycle, which is typically less than 0.3. This switching time is, however, comparable to the relaxation times of some of the phonon modes. Therefore, it is important to consider whether there is any accumulation of phonons from one switch to another. To keep the problem tractable, we ignore the device geometry completely and consider only a step-like phonon source in one dimension, as shown schematically in Fig. 11. The source is symmetric about $x=0$ where x is the coordinate direction. We place phonon sinks at $x=\pm l$.

The time dependent BTE to be solved is

$$\frac{\partial n_{\mathbf{k},s}}{\partial t} + v_x \frac{\partial n_{\mathbf{k},s}}{\partial x} = -\frac{n_{\mathbf{k},s}}{\tau_{\mathbf{k},s}} + \dot{n}_{\mathbf{k},s} f(t) \tag{29}$$

where $f(t)$ is the switching function

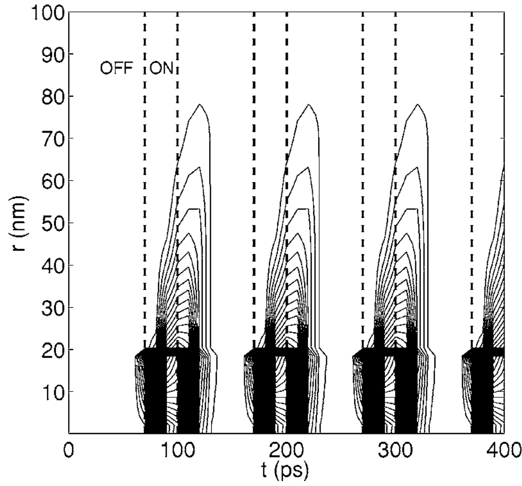

Fig. 12 Contours of the normalized phonon number density, spaced by 0.01, are shown as a function of position and time for the longitudinal optical phonon at 14 THz. No wave retardation is evident since the emitted phonons have large enough group velocities. The accumulation of LO phonons near the source during the time period of power dissipation is clearly visible.

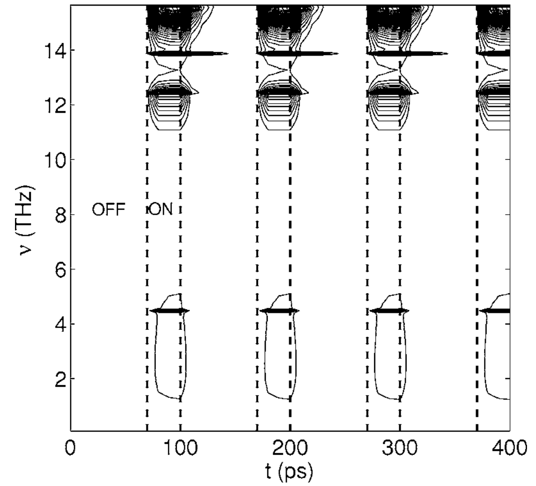

Fig. 13 Contours of the normalized phonon number density, spaced by 0.01, are shown as a function of frequency and time at x=0. There is no phonon accumulation for a switching period of 100 ps with a duty cycle of 30%.

$$
\begin{aligned}
f(t) &= 1 \quad t \bmod t_o < \alpha \\
&= 0 \quad t \bmod t_o > \alpha
\end{aligned}
\tag{30}
$$

with t_o being the switching period and α being the duty cycle or the fraction of the time period that the device is on. Further, the boundary conditions are

$$
\begin{aligned}
n^{+}_{\mathbf{k},s}(x=0,|v_x|,t) &= n^{-}_{\mathbf{k},s}(x=0,-|v_x|,t) \\
n^{-}_{\mathbf{k},s}(x=l,-|v_x|,t) &= 0 \\
T(x=l,t) &= T_o
\end{aligned}
\tag{31}
$$

where $n^{+}_{\mathbf{k},s}$ is the departure function for phonons traveling to the right in Fig. 11 and $n^{-}_{\mathbf{k},s}$ is the function for phonons traveling to the left. Equation (29) is linearized by computing the relaxation time at the temperature field obtained from the heat diffusion equation. The solution to the transient problem is

$$
\begin{aligned}
n^{+}_{\mathbf{k},s} &= e^{-\frac{x}{|v_x|\tau}}\left[\int_0^x \frac{\dot{n}}{|v_x|} f\left(t+\frac{x'-x}{|v_x|}\right) e^{\frac{x'}{|v_x|\tau}} dx' \right. \\
&\quad \left. + \int_0^l \frac{\dot{n}}{|v_x|} f\left(t-\frac{x'+x}{|v_x|}\right) e^{-\frac{x'}{|v_x|\tau}} dx'\right] \\
n^{-}_{\mathbf{k},s} &= e^{\frac{x}{|v_x|\tau}} \int_x^l \frac{\dot{n}}{|v_x|} f\left(t-\frac{x'-x}{|v_x|}\right) e^{-\frac{x'}{|v_x|\tau}} dx'
\end{aligned}
\tag{32}
$$

We now describe the numerical results for a hotspot with a power density of 5 W/μm^3. The numerical values for l, a, and the boundary temperature, T_o, used in these calculations are given in Fig. 11.

A phonon emitted during device switching may show a wave retardation in time if the time scale for switching is comparable to a characteristic time, obtained by dividing the length scale for emission by the group velocity of the emitted phonon. Retardation would cause the phonon distribution to be history dependent. In our computations, however, we do not find any evidence of retarded phonons. The spatial and temporal distribution for the 14 THz longitudinal optical phonon is shown in Fig. 12. We attribute the absence of retardation effects to the fact that phonons dominating the emission spectrum have non-zero group velocities on the order of 1000 m/s.

Another important issue is whether the switching is fast enough to cause phonons to remain in perpetually strong nonequilibrium or to even cause accumulation over time. We do not find this to be the case for typical clock cycles. This is evident from Fig. 13 which shows the number density contours at x=0 as a function of phonon frequency and switching time. The emitted phonons thermalize within the off state of the device and there is no accumulation. In the absence of phonon retardation, the accumulation of phonons from one logic state to another will only occur when the time between successive states approaches the relaxation time of the dominant LO phonons. This number is about 10 ps to the best of our knowledge. Thus, unless the switch period approaches such short times, we do not anticipate any phonon accumulation. However, we note that this assertion depends on the accuracy of the relaxation times. A detailed investigation into the accuracy of scattering rates is thus necessary before making a definitive conclusion about this aspect.

6 Concluding Remarks

In this paper, we have presented a new model for determining the non-equilibrium phonon distribution function in semiconductor devices, starting from the phonon BTE. We solved a two-dimensional form of the BTE to compare our model with previous thermal resistance data on hotspots in silicon. The thermal resistance is seen to scale as the ratio of the peak power density to the lattice heat capacity. We considered a steady-state hotspot in a 90 nm gate-length bulk silicon transistor. The source distribution is taken from our prior work on Monte Carlo simulations of electron-phonon scattering. The peak equivalent temperature rise is nearly 13% more than the temperature rise from heat diffusion, with most of the excess energy resident in longitudinal optical phonons. The solution to the transient BTE shows that the emitted phonons are able to relax completely at current switching speeds but may accumulate if the switching period is reduced by half.

We find that though ballistic transport near the hotspot introduces an additional thermal resistance to that predicted by diffusion theory, the dominating contribution to the total resistance is still from the package. The sub-continuum contribution can be significant at higher peak electric fields and current densities, both being possible in future nanotransistors. Longitudinal optical phonons dominate the emission spectrum from electron-phonon

scattering and, consequently, the energy density and heat flux at the hotspot. In a clear departure from the commonly used assumption, the dominating LO modes do not have a near-zero group velocity. Also, the mean free path of the emitted phonons is significantly shorter than that for thermal phonons at 300 K. This serves to decrease the sub-continuum size effect. Additionally, the thickness of the silicon film in a silicon-on-insulator device is important in determining the onset of sub-continuum source-size effects. For a temperature slip to occur at the heat source, the mean free path of the emitted phonons should be comparable to the film thickness. The dimension of the source plays a secondary role in determining the size effect.

We are unable to gauge the impact of sub-continuum phonon conduction on leakage currents since current methods for evaluating leakage do not account for severe nonequilibrium. This is an important area for future work. Finally, we remark that, although there has been considerable progress in techniques to solve the phonon BTE, our knowledge of phonon relaxation times at large energy densities remains poor. This, however, is a prerequisite for accurately predicting non-local effects in future transistors. The relaxation rates used in this work were all derived for near-equilibrium transport and, hence, their validity at such large excitations as near a hotspot remains unknown. The authors have investigated this aspect through molecular dynamics simulations in a separate work [22].

Acknowledgment

The authors acknowledge support from the Semiconductor Research Corporation through task 1043. S.S. was supported through graduate fellowships from the Intel Corporation and the Powell Foundation. S.S. thanks Dr. Ravi Prasher at Intel Corporation, Arizona, for helpful discussions on device boundary conditions.

References

[1] Lai, J., and Majumdar, A., 1996, "Concurrent Thermal and Electrical Modeling of Sub-Micrometer Silicon Devices," J. Appl. Phys., **79**, pp. 7353–7363.
[2] Sverdrup, P. G., Ju, Y. S., and Goodson, K. E., 2001, "Sub-Continuum Simulations of Heat Conduction in Silicon-on-Insulator Transistors," ASME J. Heat Transfer, **123**, pp. 130–137.
[3] Narumanchi, S. V. J., Murthy, J. Y., and Amon, C. H., 2004, "Submicron Heat Transport Model in Silicon Accounting for Phonon Dispersion and Polarization," ASME J. Heat Transfer, **126**, pp. 946–955.
[4] Yang, R., Chen, G., Laroche, M., and Taur, Y., 2005, "Simulation of Nanoscale Multidimensional Transient Heat Conduction Problems Using Ballistic-Diffusive Equations and Phonon Boltzmann Equation," ASME J. Heat Transfer, **127**, pp. 298–306.
[5] Sinha, S., and Goodson, K. E., 2002, "Phonon Heat Conduction From Nanoscale Hot Spots in Semiconductors," *12th International Heat Transfer Conference*, Grenoble, France.
[6] Mahan, G. D., and Claro, F., 1988, "Nonlocal Theory of Thermal Conductivity," Phys. Rev. B, **38**, pp. 1963–1969.
[7] Chen, G., 1996, "Nonlocal and Nonequilibrium Heat Conduction in the Vicinity of Nanoparticles," ASME J. Heat Transfer, **118**, pp. 539–545.
[8] Yeo, Y. C., Subramanian, V., Kedzierski, J., Xuan, P., King, T.-J., Bokor, J., and Hu, C., 2000, "Nanoscale Ultra-Thin-Body Silicon-on-Insulator P-MOSFET With a SiGe/Si Heterostructure Channel," IEEE Electron Device Lett., **21**, pp. 161–163.
[9] Klemens, P. G., 1951, "The Thermal Conductivity of Dielectric Solids at Low Temperatures—Theoretical," Proc. R. Soc. London, Ser. A, **208**, pp. 108–133.
[10] Claro, F., and Mahan, G. D., 1989, "Transient Heat Transport in Solids," J. Appl. Phys., **66**, pp. 4213–4217.
[11] Ferry, D. K., 2000, *Semiconductor Transport*, Taylor and Francis, New York.
[12] Menèndez, J., and Cardona, M., 1984, "Temperature Dependence of the First-Order Raman Scattering by Phonons in Si, Ge, and alpha-Sn: Anharmonic effects," Phys. Rev. B, **29**, pp. 2051–2059.
[13] Holland, M. G., 1963, "Analysis of Lattice Thermal Conductivity," Phys. Rev., **132**, pp. 2461–2471.
[14] Sverdrup, P. G., Sinha, S., Asheghi, M., Srinivasan, U., and Goodson, K. E., 2001, "Measurement of Ballistic Phonon Conduction Near Hot Spots in Silicon," Appl. Phys. Lett., **78**, pp. 3331–3333.
[15] Hahne, E., and Grigull, U., 1975, "Shape Factor and Shape Resistance for Steady Multidimensional Heat Conduction," Int. J. Heat Mass Transfer, **18**, pp. 751–767.
[16] Chen, G., 2001, "Ballistic-Diffusive Heat-Conduction Equations," Phys. Rev. Lett., **86**, pp. 2297–2300.
[17] Goodson, K. E., and Flik, M. I., 1992, "Effect of Microscale Thermal Conduction on the Packing Limit of Silicon-on-Insulator Electronic Devices," IEEE Trans. Compon., Hybrids, Manuf. Technol., **15**, pp. 715–722.
[18] Pop, E., Dutton, R. W., and Goodson, K. E., 2004, "Analytic Band Monte Carlo Model for Electron Transport in Silicon Including Acoustic and Optical Phonon Dispersion," J. Appl. Phys., **96**, pp. 4998–5005.
[19] Pop, E., Dutton, R. W., and Goodson, K. E., 2005, "Monte Carlo Simulations of Joule Heating in Bulk and Strained Silicon," Appl. Phys. Lett., **86**, p. 082101.
[20] Dingle, R. B., 1950, "The Electrical Conductivity of Thin Wires," Proc. R. Soc. London, Ser. A, **201**, pp. 545–560.
[21] Groeseneken, G., Colinge, J. P., Maes, H. E., Alderman, J. C., and Holt, S., 1990, "Temperature Dependence of Threshold Voltage in Thin-Film SOI MOSFETs," IEEE Electron Device Lett., **11**, pp. 329–331.
[22] Sinha, S., Schelling, P. K., Phillpot, S., and Goodson, K. E., 2005, "Scattering of *g*-Process LO Phonons at Hotspots in Silicon," J. Appl. Phys., **97**, pp. 023702.
[23] Dolling, G., 1963, "Lattice Vibrations in Crystals With the Diamond Structure," *Symposium on Inelastic Scattering of Neutrons in Solids and Liquids*, Chalk River, Canada, pp. 37–48.